Journal of Applied Physics

Weak magnetic field-dependent photoluminescence properties of lead bromide perovskites

Cite as: J. Appl. Phys. **131**, 125105 (2022); https://doi.org/10.1063/5.0085947
Submitted: 20 January 2022 • Accepted: 15 March 2022 • Published Online: 25 March 2022

Rory Butler, Randy Burns, Dallar Babaian, et al.

Journal of Applied Physics ARTICLE scitation.org/journal/jap

Weak magnetic field-dependent photoluminescence properties of lead bromide perovskites

Cite as: J. Appl. Phys. **131**, 125105 (2022); doi: 10.1063/5.0085947
Submitted: 20 January 2022 · Accepted: 15 March 2022 ·
Published Online: 25 March 2022

Rory Butler,[1] Randy Burns,[1] Dallar Babaian,[1] Matthew J. Anderson,[1] Carsten A. Ullrich,[1] Maria V. Morrell,[2] Yangchuan Xing,[2] Jaewon Lee,[2] Ping Yu,[1] and Suchismita Guha[1,a)]

AFFILIATIONS

[1]Department of Physics and Astronomy, University of Missouri, Columbia, Missouri 65211, USA
[2]Department of Chemical Engineering, University of Missouri, Columbia, Missouri 65211, USA

[a)]**Author to whom correspondence should be addressed:** guhas@missouri.edu

ABSTRACT

The strong spin–orbit coupling (SOC) in lead halide perovskites, when inversion symmetry is lifted, has provided opportunities for investigating the Rashba effect in these systems. Moreover, the strong orbital moment, which, in turn, impacts the spin-pair in singlet and triplet electronic states, plays a significant role in enhancing the optoelectronic properties in the presence of external magnetic fields in lead halide perovskites. Here, we investigate the effect of weak magnetic fields (<1 T) on the photoluminescence (PL) properties of $CsPbBr_3$ nanocrystals with and without Ruddlesden–Popper (RP) faults and single crystals of $CH_3NH_3PbBr_3$. Along with an enhancement in the PL intensity as a function of an external magnetic field, which is observed in both lead bromide perovskites, the PL emission red-shifts in $CsPbBr_3$ nanocrystals. Density-functional theory calculations of the electronic band-edge in $CsPbBr_3$ show almost no change in the energy gap as a function of the external magnetic field. The experimental results, thus, suggest the role of mixing of the triplet and singlet excitonic states under weak magnetic fields. This is further deduced from an enhancement in PL lifetimes as a function of the field in $CsPbBr_3$. In $CH_3NH_3PbBr_3$, an increase in PL intensity is observed under weak magnetic fields; however, no changes in the peak energy or PL lifetimes are observed. The internal magnetic fields due to SOC are characterized for all three samples and found to be the highest for $CsPbBr_3$ nanocrystals with RP faults.

I. INTRODUCTION

The past decade has seen a rapid development of high-performing optoelectronic applications of halide perovskite semiconductors, which share the general formula of ABX_3 with monovalent cations (A), bivalent metal cations (B), and halide anions (X). The hybrid organic-metal halide perovskites (OHPs), with A cations such as methylammonium (MA) or formamidinium (FA) and the B cation such as Pb or Sn are the front runners in photovoltaic solar cells.[1,2] Nanocrystals of all inorganic metal-halide perovskites (IHP) with Cs ions occupying the A site show tunable, narrow emission with high photoluminescence quantum yield (PLQY) making them promising candidates for next-generation displays.[3,4] The strong spin–orbit coupling (SOC) due to the presence of a heavy element (Pb) and the associated Rashba effect[5–9] make these systems relevant for spin-related device applications.[10] Additionally, the strong orbital moment arising from the lead atoms and the direct orbital bonding in the octahedra lattice provide opportunities for investigating magnetic field effects in this class of lead halide perovskites.[11]

Owing to the centrosymmetric crystal structures, the Rashba effect as such is forbidden in 3D lead halide perovskites. However, dynamic lattice distortion due to the thermal motion of the cations (MA^+, Cs^+) and local symmetry breaking due to surface defects result in Rashba splitting observed in 3D perovskite semiconductors.[12] A ramification of the Rashba effect combined with the strong SOC in the conduction band is that it lowers the bright triplet excitonic states below the dark singlet exciton in IHPs; the lowest J-triplet states in $CsPbX_3$ nanocrystals recombine 20 times faster than in any other semiconductor nanocrystals at room temperature.[13] In $CsPbBr_3$ nanocrystals, the splitting in the photoluminescence (PL) peaks at low fields was attributed to the Rashba

effect, whereas beyond 4 T the Zeeman effect was seen to be dominant.[9] Magnetic field effects (MFE), which redistribute the spin population in the presence of external magnetic fields impacting optoelectronic properties, have been the hallmark of carbon-based semiconductors where the SOC is weak.[14] The excitonic states in such semiconductors are characterized by the spin angular momentum; the equilibrium between the singlet and triplet population can, thus, be altered by an external magnetic field. Although lead halide perovskites have strong SOC, which shortens the spin relaxation times, the presence of a strong orbital moment can result in spin-mixing of the excitonic states and modulate the emission properties. The changes in PL, electroluminescence, and photocurrent response were attributed to the difference in the *g*-factors between the electron–hole pairs under magnetic field-induced spin mixing in mixed halide OHPs.[15]

Although low temperature PL including measurements under high magnetic fields has identified the nature of the lowest excitonic states in IHP[13] and OHP,[16] the effect of weak magnetic fields on the PL properties of perovskite semiconductors has not been systematically explored. In particular, the parameters describing the internal magnetic field due to SOC have not been deduced for different classes of IHP and OHP. Moreover, how this internal magnetic field may change in the presence of planar faults has not been investigated thus far.

Here, we probe the MFE in two classes of lead bromide perovskites (IHP and OHP) for field strengths <1 T. For this study, the OHP class is represented by $MAPbBr_3$ single crystals and $CsPbBr_3$ nanocrystals (defect-free and with defects) were selected for the IHP class. The demonstration of a simple post-synthesis process for introducing planar faults, namely, Ruddlesden–Popper (RP) faults, in 3D $CsPbBr_3$ nanocrystals[17] has opened up a pathway for improving the optoelectronic properties of perovskite nanocrystals. Most notably, the presence of RP faults in $CsPbBr_3$ nanocrystals enhances the PLQY,[17] demonstrates improved PL properties at 1 GPa pressure,[18] shows strong third harmonic generation,[19] and enhances the electroluminescence properties compared to $CsPbBr_3$ nanocrystals without RP faults.[20] The MFE in $CsPbBr_3$ nanocrystals manifest as enhanced PL intensity and a red-shift of the PL energy with increasing field strengths at room temperature. These changes are observed both in $CsPbBr_3$ nanocrystals with and without RP faults. The shift in the PL energy exhibits a power-law dependence on the magnetic field, which is inconsistent with the typical Zeeman energy shift or the diamagnetic term. The PL lifetime in $CsPbBr_3$ is seen to increase with the external field. The PL under hydrostatic pressure (below 1 GPa) as a function of the magnetic field was further investigated and no MFE were observed under pressure. We compare the MFE results of $CsPbBr_3$ to $MAPbBr_3$. Single crystals of $MAPbBr_3$ are known to show at least two excitonic peaks in the PL at room temperature and are sensitive to the experimental geometry—reflection or transmission. The high-energy PL peak, observed in the reflection geometry, shows a response to the magnetic field; however, the low-energy PL peak observed in the transmission geometry shows no MFE. Unlike $CsPbBr_3$, the PL lifetimes in $MAPbBr_3$ remain unchanged in the presence of the field, highlighting differences in the mixing of the singlet–triplet excitonic states between the two compounds. From the changes in the PL intensity, parameters describing the internal magnetic field due to SOC are obtained for all samples. The field is seen to be the highest for $CsPbBr_3$ nanocrystals with RP faults, which we attribute to trap/surface states.

II. METHODS

A. Materials

The synthesis of $CsPbBr_3$ nanocrystals was carried out via a hot injection method at 185 °C under N_2 atmosphere. The nanocrystals were cooled in an ice-water bath and centrifuged at 4000 rpm for 12 min. The nanocrystals were then redispersed in *n*-heptane for further analysis. The RP faults in $CsPbBr_3$ nanocrystals were developed via the addition of diethylzinc to the purified nanocrystals. The detailed procedures were reported in Refs. 17 and 20. They are also briefly discussed in supplementary material. Since there may be some batch-to-batch variation, we made sure to compare the optical properties of the non-RP and RP films from the same batch.

Methylammonium bromide, lead bromide (98%), and anhydrous dimethylformamide (DMF) were purchased from Millipore Sigma and utilized without further purification. $MAPbBr_3$ single crystals were synthesized using the inverse temperature crystallization technique as described in Ref. 21. We prepared a one molar solution of $PbBr_2$ and MABr in DMF at room temperature. The solution was stirred for an hour and then filtered through a 0.22 μm PTFE filter with the resulting filtrate distributed into vials in 2 ml portions. The vials were placed into a bath of 80 °C silicone oil for 3 h. After a short time, several nucleation sites appeared, and the crystal growth commenced. Finally, the crystals were extracted from the vials after 3 h and dried.

The $CsPbBr_3$ nanocrystals were deposited from solution onto a glass slide to form a thin film that was mounted on a non-magnetic frame for transmission geometry measurements. After each PL measurement, the excitation source was blocked to avoid photobleaching. The sample was left to relax in the magnetic field for a short period (approx. 3 min) until the next measurement. In all cases, the polarity of the magnetic field was kept constant. The high-pressure PL experiments were carried out using a Merrill–Bassett-type diamond anvil cell. A small amount of the non-RP $CsPbBr_3$ sample was dropped into the sample chamber (180 μm hole of a stainless-steel gasket) along with some silicone oil to achieve hydrostatic conditions. A small chip of ruby in the sample chamber served as the pressure calibrant.

B. Characterization

The PL measurements under magnetic fields were carried out using a 400 nm laser diode for sample excitation with a power density of 2600 W/m^2. Magnetic fields <1 T were generated by a Helmholtz coil configuration, and the field strength was modulated through adjustment of the magnetic poles and the applied voltage to the electromagnet. The magnetic field was calibrated using a kilogauss meter. The PL from $CsPbBr_3$ was measured in the transmission geometry, whereas the PL from $MAPbBr_3$ was measured in the reflection geometry. A 400 nm long pass filter separated the excitation source from the sample PL and the spectra were recorded

using a USB2000 Ocean Optics spectrometer with a 2048-pixel linear silicon CCD array.

The PL lifetimes were measured with a PicoHarp 300 time-correlated single photon counting module with 4 ps time resolution. The 800 nm wavelength (100 fs, 80 MHz) from a Ti-Sapphire laser (Mai Tai, Spectra Physics) was frequency doubled to 400 nm, which served as the excitation source using an external BBO crystal. The sample was placed in a variable gap magnet from PASCO. By changing the separation of the poles, fields up to 500 mT could be achieved. The PL decay was measured in a reflection geometry for the non-RP $CsPbBr_3$ film and the $MAPbBr_3$ crystal. The PL emission from the sample was collected by an avalanche photon counting detector module (Micro Photon Devices), using a long-pass 400 nm filter and a bandpass filter at 530 $\pm$ 10 nm to eliminate the excitation wavelength.

C. Theory

To determine the influence of magnetic fields on the electronic band structure of perovskites, we performed first-principles calculations using density-functional theory (DFT) for orthorhombic $CsPbBr_3$ in uniform magnetic fields of varying strength. The calculations were performed with ELK,[22] which is an all-electron electronic structure code (i.e., not requiring pseudopotentials). For the DFT calculations, we used the PBEsol exchange-correlation functional[23] and a $4 \times 3 \times 4$ k-point grid. The calculations were converged to a total energy tolerance of 2.7×10^{-4} eV and a total potential tolerance of 2.7×10^{-6} eV.

III. RESULTS AND DISCUSSIONS

A. Magneto-PL from $CsPbBr_3$ nanocrystals

Figures 1(a) and 1(b) compare the PL spectra from non-RP $CsPbBr_3$ and RP $CsPbBr_3$ films in a Faraday geometry as a function of the magnetic field strength. All measurements reported here are at 300 K. The individual PL spectra were fit with a Voigt profile to obtain the peak position and the intensity. Without the magnetic field, the PL peak is centered at 515 nm for the non-RP film and is slightly red-shifted at 523 nm for the RP film. The red-shift in the PL for the RP sample is expected due to the larger crystalline size; however, the shift is relatively small and does not scale with the nanocrystal size effect.[17] The insulating CsBr layers in between the $CsPbBr_3$ domains, which form the fault planes, result in a quantum confinement effect. Detailed temperature-dependent PL from non-RP and RP $CsPbBr_3$ nanocrystals showed very small shifts in the PL peak positions, consistent with a homogeneous particle size distribution.[18]

Upon increasing the magnetic field, an increase in the PL intensity along with a red-shift of the PL peak position is observed. The PL energy shifts (with respect to the zero magnetic field) are plotted in Figs. 1(c) and 1(d). The non-RP sample is seen to shift by 30 meV and the RP sample shifts by 16 meV within a range of 0.5 T. We have ensured that the red-shift in the PL is not due to any clustering effect. After switching off the field, the PL peak position was monitored for a few days. The PL peak reverts back to the original position after the field is switched off (see the supplementary material).

We note that the RP $CsPbBr_3$ sample has a broader size distribution compared to non-RP $CsPbBr_3$ (see TEM images in the supplementary material); the PL is from excitons that are quantum confined in the smaller domains within the large domains. The exciton binding energies are, in general, 20–30 meV higher in RP $CsPbBr_3$ compared to non-RP $CsPbBr_3$.[20] The change of excitonic transition energy with magnetic field, ΔE, is usually governed by two terms: the Zeeman energy, which varies linearly with the magnetic field (B), and the diamagnetic contribution, which varies as B^2. Thus, $\Delta E = \pm \frac{1}{2}\Delta g \mu_B B + c_0 B^2$, where Δg is the difference between the electron and hole g-factors, μ_B is the Bohr magneton, and c_0, the diamagnetic coefficient, depends on the excitonic Bohr radius and the effective reduced mass. The PL transition energies for both non-RP $CsPbBr_3$ and RP $CsPbBr_3$ exhibit a different behavior and do not agree with the Zeeman energy term or the diamagnetic term. Instead, we find a reasonable fit with a power law (cB^m), with m being close to 0.5. Our results are consistent with the magneto-optical measurements from single colloidal $CsPbBr_3$, which demonstrated that the Zeeman term dominates beyond 4 T[9]; hence, it is not surprising that in the range of the magnetic field in this work (<1 T), the energy shifts are not linear. The smaller coefficient, c, for RP $CsPbBr_3$ compared to non-RP $CsPbBr_3$ may be reconciled with the higher exciton binding energy in this sample.[20]

The non-linear dependence of the transition energy under weak magnetic fields exhibits some interesting features. If we take the experimental data of the PL energies vs magnetic field for the non-RP and the RP samples and add a uniform offset of 23 meV to the non-RP data, then the two datasets end up almost exactly on top of each other beyond 0.2 T (see the supplementary material). This signals two regimes: a sharp red-shift in the PL peak energy for fields lower than 0.2 T (more pronounced in the non-RP sample) along with a second region that shows a gradual change in the PL energy beyond 0.2 T. Our DFT calculations show that the magnetic fields considered in this article affect the band structure only marginally: a magnetic field of strength 1 T changes the bandgap only by about 0.1 meV. The PL red-shift observed here is, therefore, not due to any changes in the electronic structure as a function of the magnetic field.

A more plausible explanation may be due to band non-parabolicity combined with a polaronic effect. Shi *et al.*[24] observed that the PL transitions under high fields of 60 T in OHPs show inconsistent behavior across different halogen substitutions. The MFE of transition energies across various halogen substituted OHPs could not be explained by a unified model; a combination of the Rashba effect induced by strong spin–orbit coupling and the polaron effect was invoked to explain the results. According to Ref. 24, the band non-parabolicity in $MAPbI_3$ leads to a pronounced magnetic field dependence of the polaronic effective mass for field strengths below 1 T, causing shifts in the PL energy. Such a behavior has long been known for III–V semiconductors,[25] and it is likely to occur in the case of $CsPbBr_3$ as well.

The experiments in this work are conducted at room temperature where the rotation of the $PbBr_6$ lattice surrounding the Cs^+ ion occurs. The longitudinal optical (LO) phonons in polar crystals are known to result in the formation of Fröhlich polarons, which manifests as a long range interaction between the charge carrier and the phonon. The Fröhlich coupling constants for halide

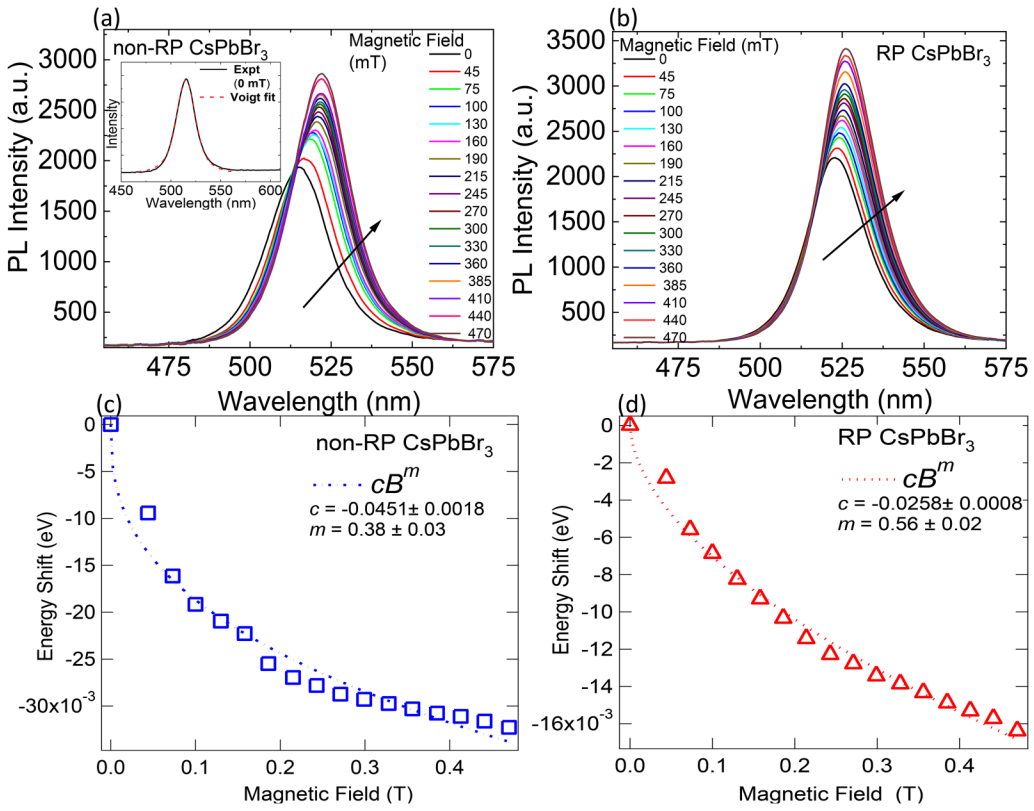

FIG. 1. PL spectra of (a) non-RP $CsPbBr_3$ and (b) RP $CsPbBr_3$ for varying magnetic fields at room temperature. The PL was measured in the transmission mode and the *B* field was aligned out of plane. The inset in (a) shows a fit to the no-field PL data with a Voigt profile. The black arrows depict increasing magnetic fields. The PL energy shift as a function of the magnetic field in (c) non-RP $CsPbBr_3$ and (d) RP $CsPbBr_3$. The dashed line in each is a fit to a power law.

perovskites are substantially larger than for inorganic semiconductors such as GaAs.[26] Angle-resolved photoelectron spectroscopy from single crystal $CsPbBr_3$ indicates parabolic bands with the evidence of large polarons resulting from an excess hole, where the polaron mass was observed to be 0.24 m_e and the polaron binding energy and radius were determined to be 34 meV and 6 nm, respectively.[27] The observed mass renormalization was ascribed to electron–phonon interaction, which is responsible for the formation of the Fröhlich polarons.[27,28] The carrier mass may be further enhanced due to the interaction with the lattice. Furthermore, the carriers may be subjected to a polar liquid-like screening[29] because of which the PL energy shifts under magnetic fields deviate from the diamagnetic term and display approximately $\sqrt{B}$ dependence.

Our prior work on high-pressure optical properties of $CsPbBr_3$ nanocrystals demonstrated a distinct red-shift of the PL energy with increasing pressure, which was consistent with DFT calculations of narrowing of the bandgap.[18] The PL as a function of the magnetic field in non-RP $CsPbBr_3$ for two values of pressure is shown in Fig. 2. The experimental geometry was identical to the ambient condition. Typical red-shift of the PL position under pressure is observed; however, as seen for the 0.3 and 0.7 GPa data, no shifts or changes in the PL intensity under pressure occur with magnetic fields. These results clearly signal an absence of MFE under pressure. We note that both PL and synchrotron-based XRD measurements under pressure from $CsPbBr_3$ show anomalies in the pressure range of 0.3–0.7 GPa, representative of an isostructural phase transition with a pressure-induced octahedral tilt.[18] Hence, we expect the relative motion between the $PbBr_6$ lattice and the Cs^+ ions to be restricted at these low pressures, reducing the dynamic and the polaronic effect, which, in turn, reduces any MFE. The locking of the A-site cation in the $MAPbX_3$ systems is, however, seen to occur at slightly higher values of pressure.[30,31]

1. Intensity changes in $CsPbBr_3$ nanocrystals

The percentage increases in the PL intensity as a function of the magnetic field in non-RP and RP $CsPbBr_3$ are shown in Fig. 3. The data were fit with the sum of two Lorentzian functions (red dashed line) of the form: $A_1[B^2/(B^2+B_1^2)] + A_2[B^2/(B^2+B_2^2)]$ and one Lorentzian function $A_1[B^2/(B^2+B_1^2)]$ (blue dotted line). Although the error bars are large for B_1 and B_2, the two Lorentzian functions fit the data far better compared to the one Lorentzian function. We will see later that this trend is different in $MAPbBr_3$. For the two Lorentzian functions, the parameters are as follow:

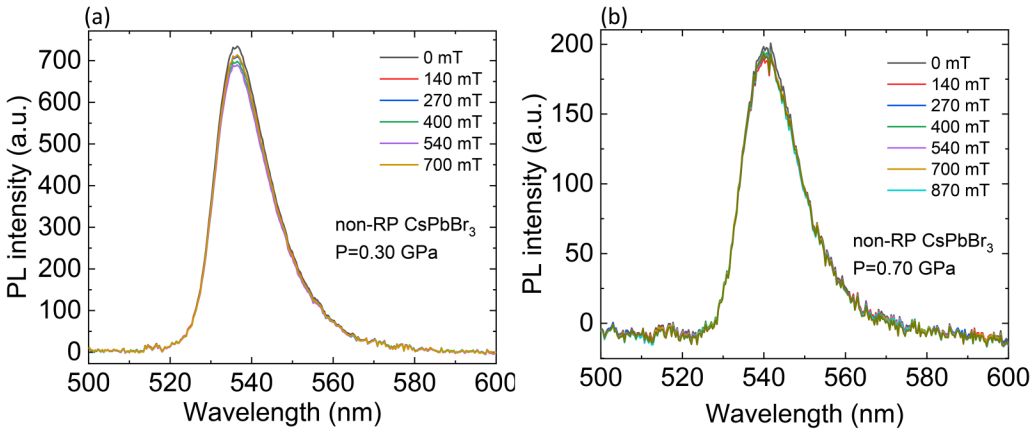

FIG. 2. PL spectra of non-RP $CsPbBr_3$ nanocrystals as a function of the magnetic field at (a) 0.30 and (b) 0.70 GPa.

$B_1 = 355 \pm 258$ mT and $B_2 = 59.0 \pm 17.5$ mT (non-RP $CsPbBr_3$) and $B_1 = 748 \pm 172$ mT and $B_2 = 65.8 \pm 6.5$ mT (RP $CsPbBr_3$).

In organic semiconductors, the fitting of MFE is usually described by two Lorentzian functions; one is related to the hyperfine interaction and the second is related to spin-exchange interactions.[32] In $CsPbBr_3$ crystals, the valence band holes show a stronger hyperfine interaction compared to conduction band electrons due to the Pb atoms.[33] In our fits, the B_2 parameter is similar for both non-RP and RP samples. This parameter is attributed to the hyperfine interaction since the composition of both samples is identical. The B_1 parameter would then represent the internal magnetic parameter, proportional to SOC.[34] Although the error bars are large in the fits, the RP sample does seem to show a somewhat larger value of B_1 compared with the non-RP sample. The differences may arise due to trap/surface states in RP-$CsPbBr_3$ at grain boundaries. We note that SOC is an atomic property and, as such, should not depend on trap states. However, the trap states are often formed as charged defects at grain boundaries in halide perovskites,[34] which may affect the local polarization and, thus, lead to consequences for the SOC. Our prior work on photon up-conversion experiments shed light on the surface states in RP-$CsPBBr_3$, which arise due to the removal of the stabilizing ligands, serving as a reservoir for the excited states.[20]

It is worth noting here that the PL intensity is seen to increase with the field, unlike in mixed halide OHPs,[15,35] where the PL intensity decreases with the application of the field. This difference is a further indication of the important role played by the lowest excitonic state: in $CsPbBr_3$, the lowest state is the triplet state,[13] whereas in the mixed OHP the lowest excitonic state is attributed to the singlet exciton.[16] This is also consistent with the MFE in organic semiconductors where both positive and negative changes in PL intensity are observed.[14] Triplet-enhanced polymers, where the decay channel between the lowest triplet and the ground state opens up, show a positive MFE beyond a certain threshold of the incident intensity,[35] similar to our observations.

We have further carried out field-induced circularly polarized PL from non-RP $CsPbBr_3$. Above 560 mT, a clear difference in intensity between σ^+ and σ^- polarized PL is observed at room temperature (see the supplementary material). A simple four-band model has been effectively used in perovskites to explain the *e-h* spin manifold and obtain insights into Δg, effective masses, and Rashba spin splitting.[14,15,36] When the field is turned on, the spin sublevels follow the Boltzmann distribution at thermal equilibrium; two of the allowed *e-h* transitions are circularly polarized since $\Delta m = \pm 1$ and the other two transitions are unpolarized since $\Delta m = \pm 0$. As a result, under thermal equilibrium, the PL intensities vary with σ^+ and σ^- due to the $\pm$ 1 values of Δm. In principle, from systematic changes in the PL intensity under σ^+ and σ^-, one should be able to deduce Δg. In our case, there are only a couple of points at higher fields where this difference is observed, and thus, Δg cannot be determined. Moreover, low temperatures are needed to deduce an accurate value of Δg. Nevertheless, our results confirm that there is spin mixing at weak magnetic fields at room temperature, which redistributes the spin population.

2. PL lifetimes under magnetic fields

Since the non-RP $CsPbBr_3$ nanocrystals do not have any additional quantum confinement effect due to fault planes, the lifetime measurements were performed only for this sample. All the legends and reference to the non-RP sample are simply referred to as $CsPbBr_3$ from here onward. To get additional insight into changes observed in magneto-PL, we measured the time-resolved PL as a function of the magnetic field. The schematic of the setup is shown in the supplementary material. A variable gap magnet was used for the application of the field. Figure 4(a) shows the PL decay curves with and without the external field. The inset shows the instrumental response function (IRF) and a fit to the 360 mT data. Since the IRF is significant here, we deconvolute the IRF and the signal (see the supplementary material) to extract the lifetimes and other parameters.

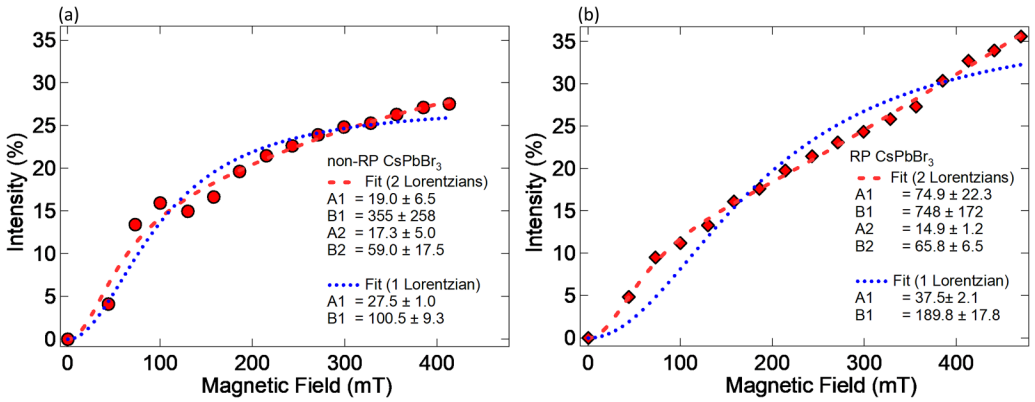

FIG. 3. The percentage increase in PL intensity as a function of the magnetic field in (a) non-RP $CsPbBr_3$ and (b) RP $CsPbBr_3$. The symbols are the experimental data, the red dashed line is a fit to two Lorentzian functions, and the blue dotted line is a fit to one Lorentzian function.

The radiative lifetimes in $CsPbX_3$ are relatively short; owing to the triplet states being the lowest optically active states, the radiative recombination decay is accelerated. The PL decay has two relaxation modes: a slow and fast one.[20] The overall decay function is of the form: $f(x) = \alpha\exp(-x/\tau_1) + \beta\exp(-x/\tau_2)$, where τ_1 and τ_2 are the two lifetimes and α and β are the components of each species. The average lifetime was obtained using $\tau_{avg} = (\alpha\tau_1^2 + \beta\tau_2^2)/(\alpha\tau_1 + \beta\tau_2)$. The decay parameters are listed in Table I. With increasing magnetic fields, the lifetime is clearly seen to increase. As shown in Fig. 4(b), the average lifetime and the fraction β/α (long to short component) both increase exponentially with the magnetic field. These results show an opposing trend to $FAPbBr_3$,[16] where the lifetime decreases with increasing field. The increasing lifetime signals a stronger mixing of the singlet–triplet states where the triplet character is enhanced.

B. Magneto-PL from $MAPbBr_3$ crystal

The PL spectra from a $MAPbBr_3$ single crystal with varying magnetic field strengths are plotted in Figs. 5(a) and 5(b) for two different geometries: reflection and transmission, respectively. It is well known that in the reflection geometry, the PL shows a dominant peak at 540 nm and a shoulder at 570 nm.[30,37,38] The appearance of the two peaks depends on the measurement geometry and the sample thickness. The sample thickness was approximately 1 mm, where self-absorption effects are typically large.[37] The low energy peak (570 nm) originates from a self-absorption effect and multiple reflections from within the bulk of the crystal. Hence, the transmission geometry mainly highlights the 570 nm peak. Changes in the PL intensity are only observed in the reflection geometry [Fig. 5(a)]. As the magnetic field strength increases, the

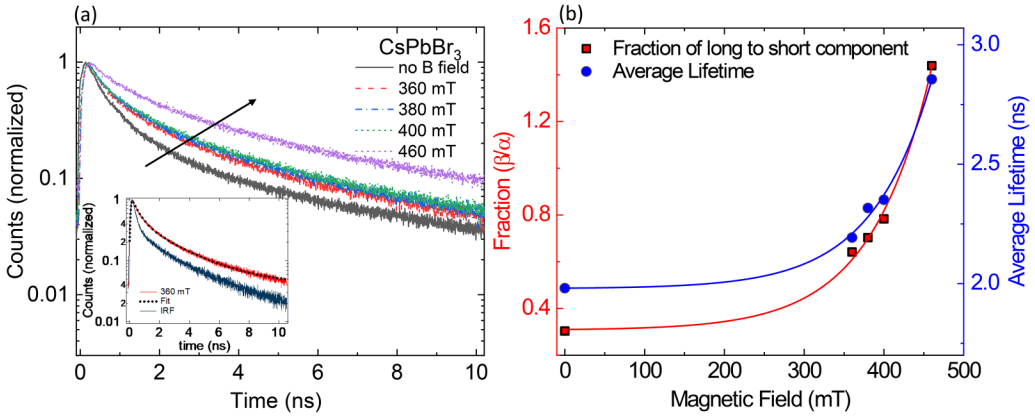

FIG. 4. (a) PL decay curves as a function of the magnetic field. The black arrow represents an increasing magnetic field. The inset shows the instrument response function and the data at 360 mT with the fitted function. (b) Ratio of β/α and the average lifetime as a function of the magnetic field. The bold lines are an exponential fit through the experimental data points.

TABLE I. Fraction of the short (α) and long (β) PL decay components along with the individual lifetimes for $CsPbBr_3$ as a function of the magnetic field. The second last column lists the average lifetime and the last column gives the β/α ratio.

Field (mT)	α	τ_1 (ns)	β	τ_2 (ns)	τ_{avg} (ns)	β/α
0	0.77	0.546 ± 0.005	0.23	2.878 ± 0.048	1.98	0.30
360	0.61	0.507 ± 0.006	0.39	2.688 ± 0.026	2.19	0.64
380	0.59	0.534 ± 0.006	0.41	2.801 ± 0.026	2.32	0.70
400	0.56	0.542 ± 0.007	0.44	2.798 ± 0.027	2.35	0.78
460	0.41	0.736 ± 0.015	0.59	3.195 ± 0.029	2.86	1.44

PL intensity increases significantly. From 0 T to 710 mT, the PL intensity increases by almost 60% with no accompanying red-shift. In the transmission geometry, however, no such change in the PL intensity with a magnetic field is observed, indicating that excitonic recombination after self-absorption in the bulk is not sensitive to external magnetic fields.

The percentage increase of PL intensity as a function of the magnetic field is plotted in Fig. 5(c). The dotted blue line is a fit with one Lorentzian function. Unlike $CsPbBr_3$, one cannot fit the enhancement in PL intensity with two Lorentzian functions, alluding to a different mechanism for MFE. The main contribution here is spin mixing induced by SOC. The fit results in the internal magnetic field parameter to be 208 ± 35 mT, a value that is close to OHP films on rigid substrates.[34] In OHPs such as $FAPbBr_3$, the dark singlet exciton state is located several meV below the bright triplet excitons.[16] We believe that it may be similar in $MAPbBr_3$, resulting in differences with $CsPbBr_3$. Unlike $CsPbBr_3$, $MAPbBr_3$ shows no change in the PL lifetime under the magnetic field [Fig. 5(d)], implying that the triplet or the singlet character of the excitons remains unchanged.

The ambient structures of $MAPbBr_3$ and $CsPbBr_3$ are different. Under ambient conditions, $MAPbBr_3$ adopts a cubic structure (space group:$Pm\bar{3}m$); both experiment and theory show that there is coupling of the MA cation to the $PbBr_6$ lattice via hydrogen bonding.[30,39] Thus, the polaron-exciton coupling may not be significant in $MAPbBr_3$, and as a result, no change in the PL energies is observed at these low magnetic fields. Furthermore, differences may also arise due to the crystal size (bulk vs nanocrystal). Electron–phonon interaction in $CsPbBr_3$ nanocrystals may be further altered due to hole self-trapping.[40]

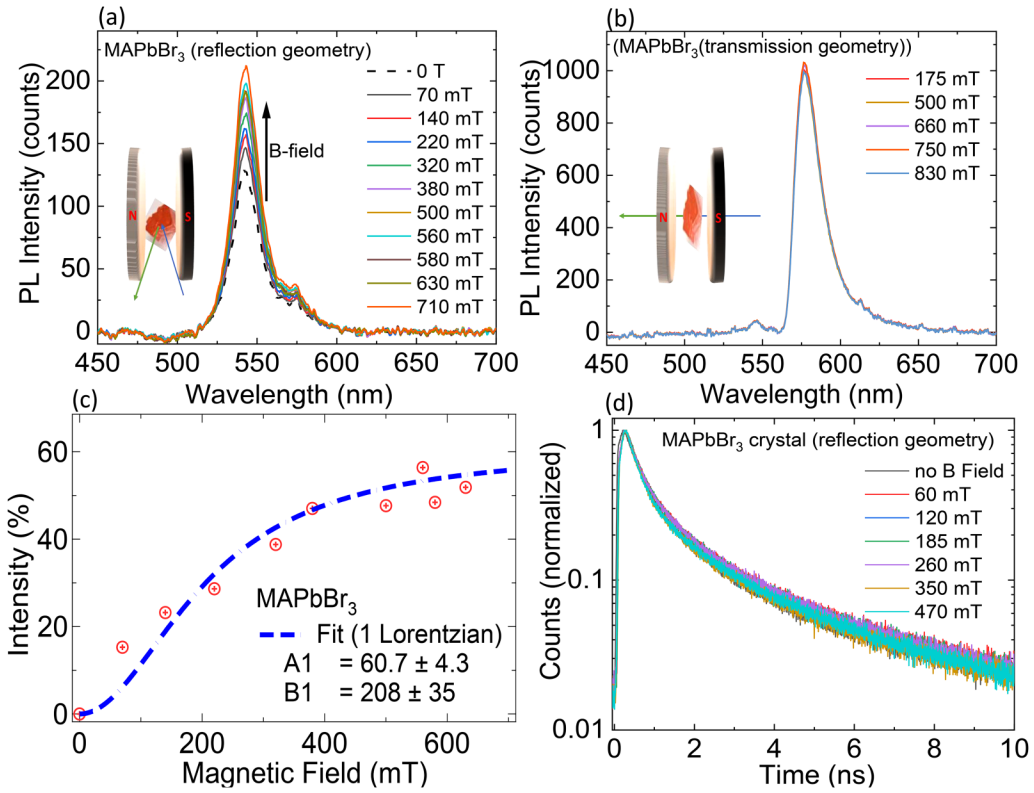

FIG. 5. PL spectra from a single crystal of $MAPbBr_3$ with varying magnetic fields in the (a) reflection and (b) transmission geometry. (c) The percentage increase in PL intensity as a function of the magnetic field. The crossed circles are the experimental data and the blue dashed line is a fit to one Lorentzian function. (d) Normalized PL decay curves for $MAPbBr_3$ as a function of magnetic field. A variable gap magnet generated the magnetic field and was aligned out of plane.

IV. CONCLUSIONS

By monitoring the PL at low magnetic fields (<1 T) for two classes of lead halide bromide perovskites, OHP ($MAPbBr_3$) and IHP ($CsPbBr_3$), the MFE was observed in both systems at room temperature. The internal magnetic field due to SOC is seen to be higher for the IHP samples, especially for RP $CSPbBr_3$, compared with $MAPbBr_3$. What is striking here is a sensitivity of the polaronic effects to weak magnetic fields at room temperature, which are highlighted in the PL properties. Although there is an absence of universality in the changes in PL energy and lifetime as a function of the magnetic field between the two bromide systems, the PL intensity is seen to increase in all samples. $CsPbBr_3$ nanocrystals with and without RP faults show a red-shift in the PL energy with the external field. This shift is inconsistent with the Zeeman energy shift or the diamagnetic term. Beyond 0.2 T, both non-RP and RP $CsPbBr_3$ show a gradual change in the PL energy. We attribute the sharp change in PL energies below 0.2 T to a polaronic effect where the carrier mass is enhanced due to the interaction with the lattice. Under high pressure and at room temperature, no change in the PL energy with the magnetic field is observed, suggesting a locking of the relative motion between the $PbBr_6$ lattice and the Cs^+ ions. The enhancement in PL intensity with the external field reflects on the SOC and the spin-mixing of triplet and singlet states, which is further gauged from the enhanced lifetimes with increasing fields. By contrast, $MAPbBr_3$ crystals show a strong enhancement in the PL intensity without any changes in the PL energy for fields up to 700 mT.

In conclusion, our study suggests that the differences in MFE between the two classes of perovskite systems can be mainly attributed to structural differences; in addition, the differences in the lowest excitonic states are likely to play a role as well. This work warrants the need for detailed theoretical models that take into account exciton-polaronic interaction to understand the MFE in these classes of halide perovskite semiconductors.

SUPPLEMENTARY MATERIAL

See the supplementary material for the synthesis of $CsPbBr_3$ nanocrystals, long-time behavior of PL signals, TEM images of RP and non-RP nanocrystals, overlaying the PL energies of the non-RP and RP samples, field-induced circularly polarized PL data, experimental setup of time-resolved PL, and deconvolution of IRF and time-resolved PL data.

ACKNOWLEDGMENTS

S.G. acknowledges the support of this work through the National Science Foundation (NSF) under Grant Nos. DMR-1807263 and ECCS-1827846. C.A.U. acknowledges support by Department of Energy under Grant No. DE-SC0019109.

AUTHOR DECLARATIONS

Conflict of Interest

The authors have no conflicts to disclose.

Author Contributions

R. Butler, R. Burns, and S. Guha conceived the experiments and carried out the photoluminescence analysis. M. V. Morrell, J. Lee, and Y. Xing involved in the synthesis of $CsPbBr_3$ nanocrystals including the introduction of RP faults. R. Burns synthesized the $MAPbBr_3$ single crystals. M. J. Anderson and C. A. Ullrich carried out the density-functional theory calculations of the electronic band-edge in $CsPbBr_3$. P. Yu, D. Babaian, and S. Guha setup the PL lifetime experiment and helped with the analysis. R. Butler and R. Burns carried out the magnetic-field-dependent photoluminescence experiments. All authors discussed and contributed to the manuscript. S. Guha, R. Burns, and C. A. Ullrich wrote and edited the manuscript.

DATA AVAILABILITY

The data that support the findings of this study are available from the corresponding author upon reasonable request.

REFERENCES

[1]A. Kojima, K. Teshima, Y. Shirai, and T. Miyasaka, "Organometal halide perovskites as visible-light sensitizers for photovoltaic cells," J. Am. Chem. Soc. **131**, 6050–6051 (2009).
[2]J. Y. Kim, J.-W. Lee, H. S. Jung, H. Shin, and N.-G. Park, "High-efficiency perovskite solar cells," Chem. Rev. **120**, 7867–7918 (2020).
[3]M. V. Kovalenko, L. Protesescu, and M. I. Bodnarchuk, "Properties and potential optoelectronic applications of lead halide perovskite nanocrystals," Science **358**, 745–750 (2017).
[4]J. Song, J. Li, X. Li, L. Xu, Y. Dong, and H. Zeng, "Quantum dot light-emitting diodes based on inorganic perovskite cesium lead halides ($CsPbX_3$)," Adv. Mater. **27**, 7162–7167 (2015).
[5]F. Zheng, L. Z. Tan, S. Liu, and A. M. Rappe, "Rashba spin-orbit coupling enhanced carrier lifetime in $CH_3NH_3PbI_3$," Nano Lett. **15**, 7794–7800 (2015).
[6]T. Etienne, E. Mosconi, and F. De Angelis, "Dynamical origin of the Rashba effect in organohalide lead perovskites: A key to suppressed carrier recombination in perovskite solar cells?," J. Phys. Chem. Lett. **7**, 1638–1645 (2016).
[7]R. B. Mohd Yusoff, A. Mahata, M. Vasilopoulou, H. Ullah, B. Hu, W. Jose da Silva, F. Kurt Schneider, P. Gao, A. V. Ievlev, Y. Liu, O. S. Ovchinnikova, F. De Angelis, and M. Khaja Nazeeruddin, "Observation of large Rashba spin-orbit coupling at room temperature in compositionally engineered perovskite single crystals and application in high performance photodetectors," Mater. Today **46**, 18–27 (2021).
[8]M. Kim, J. Im, A. J. Freeman, J. Ihm, and H. Jin, "Switchable $S = 1/2$ and $J = 1/2$ Rashba bands in ferroelectric halide perovskites," Proc. Natl. Acad. Sci. U.S.A. **111**, 6900–6904 (2014).
[9]M. Isarov, L. Z. Tan, M. I. Bodnarchuk, M. V. Kovalenko, A. M. Rappe, and E. Lifshitz, "Rashba effect in a single colloidal $CsPbBr_3$ perovskite nanocrystal detected by magneto-optical measurements," Nano Lett. **17**, 5020–5026 (2017).
[10]K. Liao, X. Hu, Y. Cheng, Z. Yu, Y. Xue, Y. Chen, and Q. Gong, "Spintronics of hybrid organic-inorganic perovskites: Miraculous basis of integrated optoelectronic devices," Adv. Opt. Mater. **7**, 1900350 (2019).
[11]K. Zhang, J. Zhao, Q. Hu, S. Yang, X. Zhu, Y. Zhang, R. Huang, Y. Ma, Z. Wang, Z. Ouyang, J. Han, Y. Han, J. Tang, W. Tong, L. Zhang, and T. Zhai, "Room-temperature magnetic field effect on excitonic photoluminescence in perovskite nanocrystals," Adv. Mater. **33**, 2008225 (2021).
[12]H. Ryu, D. Y. Park, K. M. McCall, H. R. Byun, Y. Lee, T. J. Kim, M. S. Jeong, J. Kim, M. G. Kanatzidis, and J. I. Jang, "Static Rashba effect by surface reconstruction and photon recycling in the dynamic indirect gap of $APbBr_3$ ($A = Cs, CH_3NH_3$) single crystals," J. Am. Chem. Soc. **142**, 21059–21067 (2020).

[13]M. A. Becker, R. Vaxenburg, G. Nedelcu, P. C. Sercel, A. Shabaev, M. J. Mehl, J. G. Michopoulos, S. G. Lambrakos, N. Bernstein, J. L. Lyons, T. Stöferle, R. F. Mahrt, M. V. Kovalenko, D. J. Norris, G. Rainò, and A. L. Efros, "Bright triplet excitons in caesium lead halide perovskites," Nature **553**, 189–193 (2018).
[14]H. Xu, M. Wang, Z.-G. Yu, K. Wang, and B. Hu, "Magnetic field effects on excited states, charge transport, and electrical polarization in organic semiconductors in spin and orbital regimes," Adv. Phys. **68**, 49–121 (2019).
[15]C. Zhang, D. Sun, C. X. Sheng, Y. X. Zhai, K. Mielczarek, A. Zakhidov, and Z. V. Vardeny, "Magnetic field effects in hybrid perovskite devices," Nat. Phys. **11**, 427–434 (2015).
[16]P. Tamarat, M. I. Bodnarchuk, J.-B. Trebbia, R. Erni, M. V. Kovalenko, J. Even, and B. Lounis, "The ground exciton state of formamidinium lead bromide perovskite nanocrystals is a singlet dark state," Nat. Mater. **18**, 717–724 (2019).
[17]M. V. Morrell, X. He, G. Luo, A. S. Thind, T. A. White, J. A. Hachtel, A. Y. Borisevich, J.-C. Idrobo, R. Mishra, and Y. Xing, "Significantly enhanced emission stability of $CsPbBr_3$ nanocrystals via chemically induced fusion growth for optoelectronic devices," ACS Appl. Nano Mater. **1**, 6091–6098 (2018).
[18]S. Yesudhas, M. V. Morrell, M. J. Anderson, C. A. Ullrich, C. Kenney-Benson, Y. Xing, and S. Guha, "Pressure-induced phase changes in cesium lead bromide perovskite nanocrystals with and without Ruddlesden–Popper faults," Chem. Mater. **32**, 785–794 (2020).
[19]P. Bhattacharya, M. V. Morrell, Y. Xing, C. J. Mathai, P. Yu, and S. Guha, "Enhanced third harmonic generation in lead bromide perovskites with Ruddlesden–Popper planar faults," J. Phys. Chem. Lett. **12**, 4092–4097 (2021).
[20]M. V. Morrell, A. Pickett, P. Bhattacharya, S. Guha, and Y. Xing, "Inorganic Ruddlesden–Popper faults in cesium lead bromide perovskite nanocrystals for enhanced optoelectronic performance," ACS Appl. Mater. Interfaces **13**, 38579–38585 (2021).
[21]M. I. Saidaminov, A. L. Abdelhady, B. Murali, E. Alarousu, V. M. Burlakov, W. Peng, I. Dursun, L. Wang, Y. He, G. Maculan, A. Goriely, T. Wu, O. F. Mohammed, and O. M. Bakr, "High-quality bulk hybrid perovskite single crystals within minutes by inverse temperature crystallization," Nat. Commun. **6**, 7586 (2015).
[22]J. K. Dewhurst *et al.*, "The Elk Code," see http://elk.sourceforge.net/ (2004).
[23]J. P. Perdew, A. Ruzsinszky, G. I. Csonka, O. A. Vydrov, G. E. Scuseria, L. A. Constantin, X. Zhou, and K. Burke, "Restoring the density-gradient expansion for exchange in solids and surfaces," Phys. Rev. Lett. **100**, 136406 (2008).
[24]Y. H. Shin, H. Choi, C. Park, D. Park, M. S. Jeong, H. Nojiri, Z. Yang, Y. Kohama, and Y. Kim, "Combination of optical transitions of polarons with Rashba effect in methylammonium lead trihalide perovskites under high magnetic fields," Phys. Rev. B **104**, 035205 (2021).
[25]E. D. Palik, G. S. Picus, S. Teitler, and R. F. Wallis, "Infrared cyclotron resonance in InSb," Phys. Rev. **122**, 475–481 (1961).
[26]Y. Yamada, H. Mino, T. Kawahara, K. Oto, H. Suzuura, and Y. Kanemitsu, "Polaron masses in $CH_3NH_3PbX_3$ perovskites determined by Landau level spectroscopy in low magnetic fields," Phys. Rev. Lett. **126**, 237401 (2021).
[27]M. Puppin, S. Polishchuk, N. Colonna, A. Crepaldi, D. N. Dirin, O. Nazarenko, R. De Gennaro, G. Gatti, S. Roth, T. Barillot, L. Poletto, R. P. Xian, L. Rettig, M. Wolf, R. Ernstorfer, M. V. Kovalenko, N. Marzari, M. Grioni, and M. Chergui, "Evidence of large polarons in photoemission band mapping of the perovskite semiconductor $CsPbBr_3$," Phys. Rev. Lett. **124**, 206402 (2020).
[28]C. M. Iaru, J. J. Geuchies, P. M. Koenraad, D. Vanmaekelbergh, and A. Y. Silov, "Strong carrier-phonon coupling in lead halide perovskite nanocrystals," ACS Nano **11**, 11024–11030 (2017).
[29]K. Miyata, T. L. Atallah, and X.-Y. Zhu, "Lead halide perovskites: Crystal-liquid duality, phonon glass electron crystals, and large polaron formation," Sci. Adv. **3**, e1701469 (2017).
[30]S. Yesudhas, R. Burns, B. Lavina, S. N. Tkachev, J. Sun, C. A. Ullrich, and S. Guha, "Coupling of organic cation and inorganic lattice in methylammonium lead halide perovskites: Insights into a pressure-induced isostructural phase transition," Phys. Rev. Mater. **4**, 105403 (2020).
[31]A. Francisco-López, B. Charles, O. J. Weber, M. I. Alonso, M. Garriga, M. Campoy-Quiles, M. T. Weller, and A. R. Goñi, "Pressure-induced locking of methylammonium cations versus amorphization in hybrid lead iodide perovskites," J. Phys. Chem. C **122**, 22073–22082 (2018).
[32]L. He, M. Li, A. Urbas, and B. Hu, "Magnetophotoluminescence line-shape narrowing through interactions between excited states in organic semiconducting materials," Phys. Rev. B **89**, 155304 (2014).
[33]V. V. Belykh, D. R. Yakovlev, M. M. Glazov, P. S. Grigoryev, M. Hussain, J. Rautert, D. N. Dirin, M. V. Kovalenko, and M. Bayer, "Coherent spin dynamics of electrons and holes in $CsPbBr_3$ perovskite crystals," Nat. Commun. **10**, 1–6 (2019).
[34]Q. Zhang, H. Yu, F. Zhao, L. Pei, J. Li, K. Wang, and B. Hu, "Substrate-dependent spin-orbit coupling in hybrid perovskite thin films," Adv. Funct. Mater. **29**, 1904046 (2019).
[35]Y.-C. Hsiao, T. Wu, M. Li, and B. Hu, "Magneto-optical studies on spin-dependent charge recombination and dissociation in perovskite solar cells," Adv. Mater. **27**, 2899–2906 (2015).
[36]Z. G. Yu, "Effective-mass model and magneto-optical properties in hybrid perovskites," Sci. Rep. **6**, 28576 (2016).
[37]Y. Fang, H. Wei, Q. Dong, and J. Huang, "Quantification of re-absorption and re-emission processes to determine photon recycling efficiency in perovskite single crystals," Nat. Commun. **8**, 14417 (2017).
[38]T. Thu Ha Do, A. Granados del Águila, C. Cui, J. Xing, Z. Ning, and Q. Xiong, "Optical study on intrinsic exciton states in high-quality $CH_3NH_3PbBr_3$ single crystals," Phys. Rev. B **96**, 075308 (2017).
[39]J.-H. Lee, N. C. Bristowe, J. H. Lee, S.-H. Lee, P. D. Bristowe, A. K. Cheetham, and H. M. Jang, "Resolving the physical origin of octahedral tilting in halide perovskites," Chem. Mater. **28**, 4259–4266 (2016).
[40]A. J. Neukirch, W. Nie, J.-C. Blancon, K. Appavoo, H. Tsai, M. Y. Sfeir, C. Katan, L. Pedesseau, J. Even, J. J. Crochet, G. Gupta, A. D. Mohite, and S. Tretiak, "Polaron stabilization by cooperative lattice distortion and cation rotations in hybrid perovskite materials," Nano Lett. **16**, 3809–3816 (2016).